Structural and magnetic characterization of 3*d* metal clusters embedded in fullerite matrices

C.M. Teodorescu[*], D. Macovei[*], A. Lungu[*], and G. van der Laan[**]

[*]National Institute of Materials Physics Bucharest, P.O. Box MG-7, 077125 Magurele-Ilfov Romania
[**]Magnetic Spectroscopy, Daresbury Laboratory, Warrington Cheshire WA4 4AD United Kingdom

ABSTRACT

Ni clusters are synthesized into well-ordered *fcc* fullerite (C_{60}) matrices by vacuum co-evaporaton at various relative concentrations of metal and fullerene. The samples are subsequently analyzed by X-ray diffraction (XRD), extended X-ray absorption fine structure (EXAFS), X-ray absorption near-edge structure (XANES), and X-ray magnetic circular dichroism (XMCD). XRD analysis revealed nanosized particles with average diameters ranging from 5 to 20 nm, depending on the synthesis conditions. The fullerite matrix exhibits long-range order. EXAFS is used to derive the local atomic ordering, whereas the pre-edge peak in XANES were used to quantify the depletion of metal 3*d* states due to the charge transfer from metal to surrounding fullerenes. The magnetic measurements reveal novel properties, such as the co-existence of two Ni sites, with antiferromagnetic coupling - most probably, attributed to surface and bulk atoms.

Keywords: nickel clusters, fullerene, EXAFS, XANES, XMCD

1 INTRODUCTION

Continuous effort has been dedicated over the last decades to enhance the storage density of magnetic recording media. Materials formed by highly-dispersed metal nanoparticles seem very promising [1-3]. A few years ago, Ref. [3] reported the synthesis of such nanostructured materials by co-deposition of metals with fullerene (C_{60}) molecules. These metal nanoparticles embedded in fullerite matrix present unique features desirable for magnetic recording media: strong coercitive fields and perpendicular magnetic anisotropy, resulted from the columnar shape of the nanoparticles. These metal clusters have also an increased resistance to oxidation [3,4]. Generally, structures formed between metals and C_{60}: interfaces [5,6], multilayers [7], and metals embedded in C_{60} [8,9], are subject of a continuous interest.

Fe and Co clusters embedded in C_{60} were reported in Ref. [3]. In the following, we will present investigations on structure and magnetism of Ni/C_{60}. Although in free clusters Ni presents an enhanced atomic magnetic moment of up to 1.1 μ_B [10], for Ni clusters embedded in AlN matrices, the atomic magnetic moment decreases due to the formation of a magnetically dead layer at the cluster interface with the matrix [11]. In fullerene, due to the charge transfer between Ni and C_{60} of 2*e* [5], the Ni 3*d* band is expected to deplete and this could give an increase of the magnetic moment.

We shall emphasize unique features presented by nanostructured Ni/C_{60}, particularly the anti-ferromagnetically ordered surface and bulk moments, with a very large value of the orbital moment for the surface atoms.

2 EXPERIMENTAL

Ni/C_{60} thin films were grown by co-deposition of nickel and C_{60} [3,9] onto Si or SiO_2 substrates, at National Institute of Materials Physics Bucharest. Ni was evaporated from an electron bombardment source (4 kV, 200 mA), and C_{60} is sublimated from a Knudsen cell at temperatures of 420-490 ^{o}C. The deposition rates, in the range of 1-2 nm/min, are calibrated using a quartz microbalance. The Ni content, as determined by energy dispersive X-ray spectroscopy (EDX), ranges between 75 and 0.2 at. %. The substrate temperature was controlled. The pressure during deposition is 3×10^{-5} mbar. Following the co-deposition stage, some 2-3 nm of C_{60} are deposited on top to prevent oxidation. Finally, the samples are removed from the vacuum chamber for transfer to synchrotron radiation centers.

X-ray diffraction (XRD) was measured on beamline DW22 at the DCI storage ring of the LURE synchrotron radiation facility in Orsay, France. X-ray absorption fine structure (EXAFS and XANES) was measured on beamline D43 (EXAFS4) at the same storage ring facility (DCI, Orsay). Ni $L_{2,3}$ X-ray magnetic circular dichroism was measured in magnetic fields of ± 0.6 T, by using the Flipper chamber [12] on beamline 1.1 (75 % circularly polarized light) at Daresbury Laboratory, Warrington, UK.

3. RESULTS AND DISCUSSIONS

3.1. X-ray diffraction

Figure 1 present θ - 2θ XRD scans on several samples. The photon wavelength is fixed, equal to 1.0736 Å. The sample with the most concentrated Ni content (P1, with 75 at. % Ni) shows no contribution from the C_{60} matrix. The other samples present broadened Ni [(111), (200), and

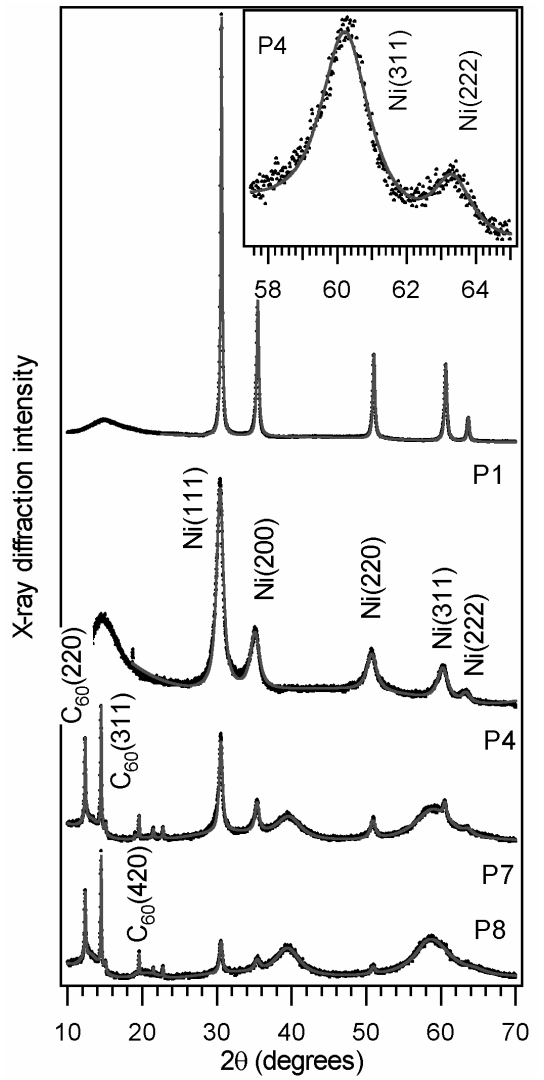

Figure 1: X-ray diffraction of selected co-deposited Ni-fullerene thin films. Insert: detail comparing the experimental data and the deconvolution in the Ni(311) - Ni(222) range of sample P4.

(220)] diffraction lines simultaneously with the fullerite diffraction features [(111), (220), (311), (420), (422), and (511)] in the range of $2\theta = 7 - 25^{o}$. This is a first interesting result, since in previous work (e.g. Ref. [13]), co-deposition of nickel and fullerenes resulted in nickel granular films embeded in amorphous carbon. The Ni diffraction peaks are deconvoluted using Voigt profiles [14] to separate the Lorentzian contribution, ascribed to the limited coherence length [9], from the Gaussian contribution, which is related to the monochromator bandwidth and to the average lattice distortions. As can be seen from the insert of Fig. 1, the quality of the deconvolution is satisfactory. The Lorentzian angular width of the lines, β (in radians), is connected to the average nanoparticle size D by using Scherrer's equation $D \approx 0.9\ \lambda / (\beta \cos \theta)$. The results obtained for D are summarized in Table 1. One may observe that the average particle size ranges between 19 nm (sample P1) and 5.8 nm (sample P7) for the samples presented in this work.

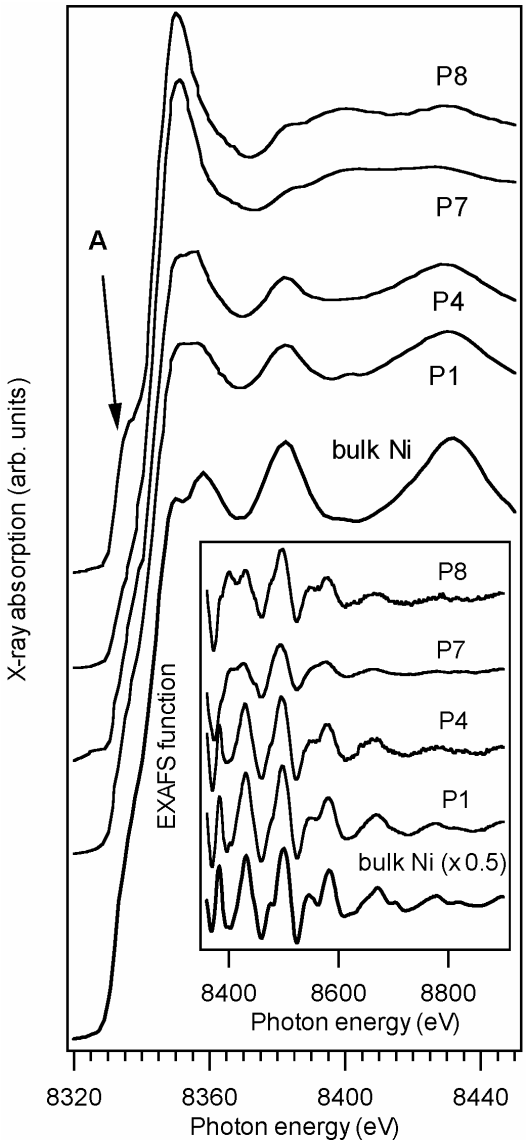

Figure 2: X-ray absorption near-edge structure (XANES) at the nickel K-edge in selected nickel-fullerene thin films. The insert represents the Extended X-ray absorption fine structure (EXAFS) region.

3.2. X-ray absorption fine structure

Figure 2 presents the X-ray absorption near-edge structure (XANES) spectra recorded at the Ni K-edge on the samples discussed previously. One may remark that the XANES features evolve gradually from a spectrum quite similar to that of bulk *fcc* Ni to a spectrum more characteristic to Ni compounds. At the same time, the pre-edge peak, which is a sign of dipole forbidden $1s \rightarrow 3d$ transitions, increases in intensity. We estimated the integral

NSTI-Nanotech 2007, www.nsti.org, ISBN 1420061828 Vol. 1, 2007

intensity of this pre-edge peak and compared it with the intensity of this peak in the Ni K-edge of NiO, where the number of Ni 3*d* holes is close to two. Therefore, this gives an estimate on the average charge transfer from the Ni clusters to the surrounding C_{60}. The results are in line with the average particle sizes derived by XRD, by assuming that surface Ni atoms transfer to the fullerene around +2*e*, result in agreement with reported data from literature [5]. We remark also that, at least for samples P1 and P4, the XANES spectrum close to that of Ni metal suggest that nanoparticles in fullerene are protected against oxydation.

Figure 2 represents the Fourier transforms (FT) of the *k*-weighted EXAFS functions for samples of interest, after standard data analysis [15]. Within the investigated samples, one may see the gradual occurence of maxima in the FT corresponding to Ni-C bonds, and as well Ni-Ni bonds in nickel carbide (Ni_3C). This result also agrees with the derived reduction of nanoparticle average size and 3*d* state depletion.

Table 1: Relevant parameters of investigated samples: the substrate temperature (T_s), the average nanoparticle size (D), the value of the average 3*d* depletion of the nickel density of states (Δn_h^{3d}), the orbital (m_l) and spin (m_s) moments for a Ni atom.

Sample	T_s (ºC)	D (nm)	Δn_h^{3d}	m_l (μ_B)	m_s (μ_B)
P1	195±5	19.2±1.3	~ 0.0	0.014	0.493
P4	140±17	6.8±0.4	~0.2 e	0.014	0.223
P7	135±15	5.8±0.7	~0.3 e	0.000	0.025
P8	105±25	9.7±1.1	1±0.1e	- 0.025	0.052

3.3. X-ray magnetic circular dichroism

Figure 4 presents X-ray magnetic circular dichroism (XMCD) measurements at Ni $L_{2,3}$ edges. Signals for samples P1 and P4 are quite similar to the "normal" Ni XMCD signal [16], whereas for samples P7 and P8 the XMCD presents anomalous derivative-like features, which may be attributed to two chemically-shifted contributions of opposite signs. The simplest interpretation is to suppose that one component corresponds to bulklike Ni and the second component to surface Ni atoms. The "surface" component is shifted with respect to the bulk component by $\Delta E = 0.88 \pm 0.02$ eV.

XMCD sum rules [16,17] were applied to derive the orbital and spin moments. The obtaines results are tabulated in Table 1. By assuming that the Ni nanoparticles are nearly spherical, the ratio between surface and bulk atoms can be expressed as $N_{surface} / N_{bulk} \approx 6d/D$, where d is close to the Ni-Ni interatomic distance. By considering that the observed values are contributions from the bulk and surface atoms, with antiferromagnetic ordering, one obtains the following values for the Ni surface and bulk moments: $m_{s,\ surface} = -0.567\ \mu_B$, $m_{l,\ surface} = -0.045\ \mu_B$, $m_{s,\ bulk} = 0.303\ \mu_B$, and $m_{l,\ bulk} = 0.003\ \mu_B$ (errors: ± 20%) [18]. Consequently, the spin bulk moment is lower than in bulk *fcc* Ni (0.67 μ_B), whereas at the surface the orbital moment increases dramatically. As soon as the particle size decreases, the (essentially) spin moment also decreases drastically. The surface component has a huge orbital moment, exceeding the spin moment by a factor of 2.2 - 2.3. Such increase in the orbital moment was already reported for nanoscale Fe clusters [19]; however, in the present case the increase is much higher. The above values were obtained with the value of n_h for bulk Ni. In presence of a charge transfer from the Ni clusters to the C_{60} matrix, a larger value of the number of 3*d* holes has to be considered, yielding even greater values of orbital moments for the surface component.

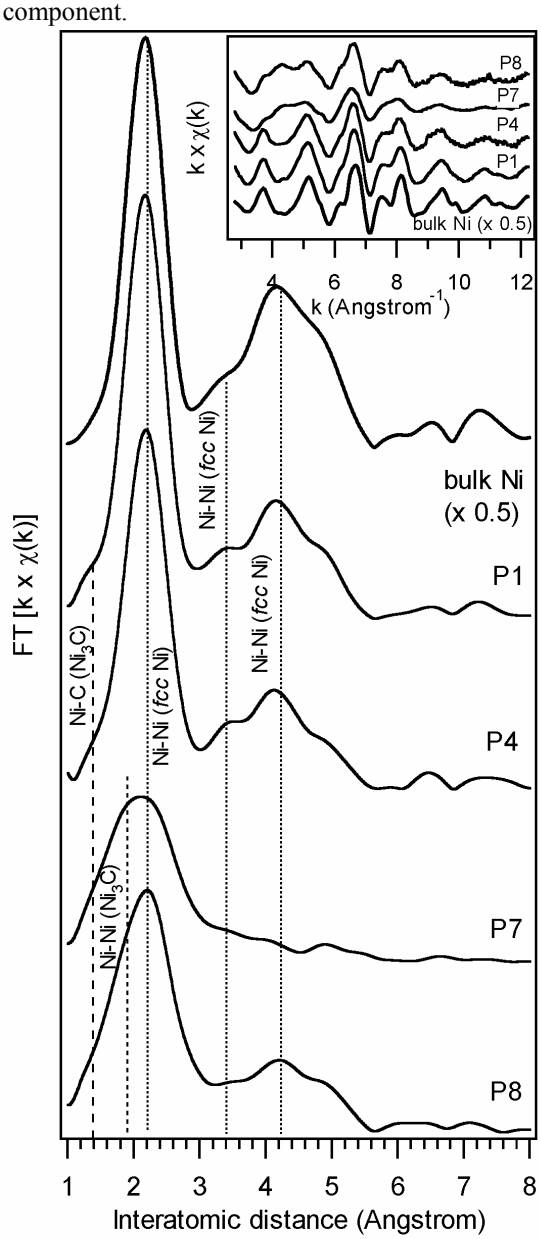

Figure 3: Fourier transforms of the EXAFS functions, weighted by the photoelectron wavevector *k*. The insert represents the same EXAFS functions as from the insert of Fig. 2, but weighted by *k*.

4 CONCLUSION

Summarising, nanostructured Ni clusters in C_{60} matrices produced by metal and fullerene co-evaporation in vacuum were investigated by X-ray magnetic circular dichroism, correlated with nanoparticle structural measurements by X-ray diffraction and by X-ray absorption fine structure. We have shown Ni nanoparticle formation dispersed in a relatively ordered *fcc* C_{60} matrix. The Ni clusters show the unique feature of antiferromagnetic coupling between bulk Ni atoms and surface Ni atoms, which are localized at the interface with the fullerite matrix. Also, the orbital magnetic moment for interface Ni atoms is strongly increased with respect to the bulk Ni atoms. We hope that these results will stimulate theoretical effort in nanoparticle magnetism.

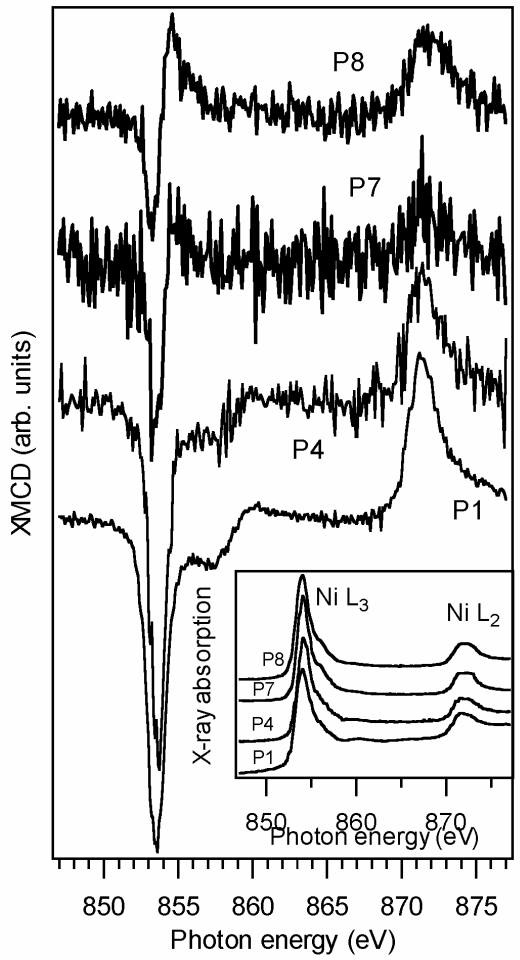

Figure 4: X-ray magnetic circular dichroism (XMCD) for the selected samples. The insert represents the isotropic absorption at the Ni $L_{2,3}$ -edges.

Acknowledgements: This work was supported the Romanian National Authority for Research through Contract CEx05-D11-32. We acknowledge great help from Dr. Agnes Traverse and Dr. Erik Elkaim from LURE.

REFERENCES

[1] N. Grobert, W.K. Hsu, Y.Q. Zhu, J.P. Hare, H.W. Kroto, D.R.M. Walton, M. Terrones, H. Terrones, P. Redlich, M. Rühle, R. Escudero, and F. Morales, Appl. Phys. Lett. **75**, 3363 (1999).
[2] Y. Yoshida, S. Shida, T. Ohsuna, and N. Shiraga, J. Appl. Phys. **76**, 4533 (1994); S. Seraphin, D. Zhou and J. Jiao, J. Appl. Phys. **80**, 2097 (1996).
[3] L.A. Zheng, B.M. Lairson, E.V. Barrera, and R.D. Shull, Appl. Phys. Lett. **77**, 3242 (2000).
[4] K.W. Edmonds, S.H. Baker, S.C. Thornton, M.J. Maher, A.M. Keen, and C. Binns, J. Appl. Phys. **86**, 2651 (1999).
[5] M.R.C. Hunt, S. Modesti, P. Rudolf, and R.E. Palmer, Phys. Rev. B **51**, 10039 (1995).
[6] C. Cepek, A. Goldoni and S. Modesti, Phys. Rev. B **53**, 7466 (1996).
[7] A.F. Hebard, R.R. Ruel and C.B. Eom, Phys. Rev. B **54**, 14052 (1996).
[8] J.G. Hou, Y. Wang, W. Xu, S.Y. Zhang, Z. Jian, and Y.H. Zhang, Appl. Phys. Lett. **70**, 3110 (1997); A. Devenyi, R. Manaila, A. Belu-Marian, D. Macovei, M. Manciu, E.M. Popescu, M. Tanase, D. Fratiloiu, N.D. Mihai, P.B. Barna, J. Labar, G. Safran, A. Kovacs, and T. Braun, Thin Solid Films **335**, 258 (1998); R. Manaila, A. Belu-Marian, D. Macovei, G. Brehm, D. T. Marian, and I. Baltog, J. Raman Spectrosc. **30**, 1019 (1999).
[9] R. Popescu, D. Macovei, A. Devenyi, R. Manaila, P.B. Barna, A. Kovacs, and J.L. Lábár, Eur. Phys. J. B **13**, 737 (2000).
[10] I.M.L. Billas, A. Châtelain and W.A. de Heer, Science **265**, 1682 (1994).
[11] D. Zanghi, C.M. Teodorescu, F. Petroff, H. Fischer, C. Bellouard, C. Clerc, C. Pélissier, and A. Traverse, J. Appl. Phys. **90**, 6367 (2001).
[12] E. Dudzik, G. van der Laan and S.M. Thompson, Synchrotron Radiation News **13**, 18 (2000).
[13] Z. Zhao, H. Wang, B. Wang, J.G. Hou, G.L. Liu, and X.F. Jin, Phys. Rev. B **65**, 235413 (2002).
[14] C.M. Teodorescu, J.M. Esteva, R.C. Karnatak, and A. El Afif, Nucl. Instrum. Meth. Phys. Res. A **345**, 141 (1994).
[15] B.K. Teo, *EXAFS: Basic Principles and Data Analysis*, Springer, Berlin (1983).
[16] C.T. Chen, Y.U. Idzerda, H.-J. Lin, N.V. Smith, G. Meigs, E. Chaban, G.H. Ho, E. Pellegrin, and F. Sette, Phys. Rev. Lett. **75**, 152 (1995).
[17] B.T. Thole, P. Carra, F. Sette, and G. van der Laan, Phys. Rev. Lett. **68**, 1943 (1992); P. Carra, B.T. Thole, M. Altarelli, and X. Wang, Phys. Rev. Lett. **70**, 694 (1993).
[18] C.M. Teodorescu, D. Macovei, and A. Lungu, J. Optoel. Adv. Mater. **6**, 1275 (2004).
[19] J. Lindner, P. Poulopoulos, F. Wilhelm, M. Farle, and K. Baberschke, Phys. Rev. B **62**, 10431 (2000).